SIAM J. APPL. MATH.
Vol. 51, No. 6, pp. 1556-1567, December 1991

005

A SOLUTION TO THE SCATTERING OF ELECTROMAGNETIC WAVES FROM A DIELECTRIC SEMI-CYLINDER*

A. K. GAUTESEN†, R. W. ZIOLKOWSKI‡, AND R. R. McLEOD‡

Abstract. The problem of scattering of electromagnetic waves from an arbitrary, infinite dielectric semi-cylinder is treated analytically through a combined dual series and integral equation formulation. It is demonstrated that the numerical implementation of this treatment satisfies the reciprocity relation as well as the electromagnetic boundary conditions. Numerical results are also provided to illustrate the fields generated in the vicinity of the semi-cylinder directly and in the far-field indirectly through the use of radar cross sections.

Key words. electromagnetic waves, scattering, diffraction, dual series, dielectric semi-cylinder

AMS(MOS) subject classifications. 35J05, 78A45

1. Introduction.

The class of electromagnetic scattering problems dealing with dielectrics that have known solutions is rather limited. Most general textbooks treat scattering from a dielectric cylinder and a dielectric sphere as the basic cases. However, with the current interest in low observable technology, the need for canonical problems dealing with dielectrics in the presence of edges has increased dramatically.

We study the problem of scattering of electromagnetic waves from an infinite dielectric semi-cylinder. This problem deals with a scattering object that intrinsically has edges which become expressed physically as singularities in the transverse field components. Canonical problems of this type are quite important for studying the basic scattering physics and for acting as benchmarks for approximate and numerical methods, especially those dealing with edge conditions. Moreover, because the electromagnetic boundary conditions are satisfied for arbitrary dielectric parameters across the various dielectric regions (dielectric semi-cylinder, complementary semi-cylinder, and exterior to either semi-cylinder), we can use this problem to study the transition from a complete dielectric cylinder to the present semi-cylinder case. This will provide valuable information to those dealing with object identification problems.

We begin our analysis from a potential formulation point of view. We assume that the incident field orginates from a magnetic line source parallel to the axis of the semi-cylinder so that the electromagnetic field problem reduces to a two-dimensional one dealing only with the H_z, E_r, and E_θ field components and a point source. We also assume the source is time-harmonic so that the problem further reduces to a Helmholtz equation for the potential u representing the H_z field component, plus its boundary conditions. The problem is then divided into a symmetric problem and an antisymmetric problem by placing another source with the appropriate sign at the location of the image about the axis of symmetry of the applied source. In this work we consider only the symmetric problem. When the applied source is located on the axis of symmetry, the problem reduces to a symmetric one. The numerical results

* Received by the editors October 10, 1989; accepted for publication (in revised form) October 11, 1990. This work was performed in part under the auspices of the U.S. Department of Energy, by the Lawrence Livermore National Laboratory, Livermore, California 94550, under contract W-7405-ENG-48.

† Ames Laboratory and Department of Mathematics, Iowa State University, Ames, Iowa 50011. The work of this author was supported in part by the Applied Mathematical Sciences subprogram of the Office of Energy Research, U.S. Department of Energy, contract W-7405-ENG-82.

‡ Engineering Research Division, Lawrence Livermore National Laboratory, Livermore, California 94550.

presented are for this restricted case. The antisymmetric problem can be dealt with by a method similar to the one used for the symmetric problem. The source is also assumed to lie outside the cylinder which contains the dielectric half-cylinder.

Space is divided into three regions: the region occupied by the dielectric half-cylinder, the complementary half-cylinder, and the remaining exterior region. In the first two regions, the fields are expanded in a series of functions which satisfy the appropriate Helmholtz equation and the boundary conditions on the plane wall of the dielectric half-cylinder (see (2.9) and (2.10) below). In the last region the field is expanded in a series of functions which satisfy the appropriate Helmholtz equation and the radiation bundary condition at infinity (see (2.11) below). The remaining boundary conditions on the cylindrical boundary lead to a dual series equation set (see (2.20) and (2.21) below). They contain two sets of unknown coefficients, $\{a_j\}$ and $\{b_j\}$.

The complexity of the dual series equation set makes a completely analytical solution unlikely. Thus some numerical analysis is required. If we simply truncate these series, the resulting set of equations has a poorly conditioned matrix, which makes its solution problematic. It is suspected that this is caused by the singularities at the dielectric corners. The left sides of (2.20) and (2.21) are the dual series equation set corresponding to the static problem. The static problem is, of course, governed by Laplace's equation (instead of Helmholtz's equation) and the same boundary conditions on the dielectric half-cylinder. The static semi-cylinder problem also is apparently unsolved. Its solution is found here, and it gives the correct singularities at the corners (see, e.g., [3]–[5]).

Operating on the dual series equation set (2.20) and (2.21) with the inverse of the static problem leads to the dual series equation set (4.1) and (4.2). It is this system of equations that is numerically analyzed. The matrix M_{ij} of this system of equations numerically appears to behave like the Kronecker delta for values of its indices sufficiently large, i.e., $M_{ij} \sim \delta_{ij}$ for $i > N$ and $j > N$. Thus the system of equations is truncated and the resulting set of equations is inverted. As a test of the accuracy of this approximation, the principle of reciprocity is used. This principle states that the field u of the field point $\mathbf{r}$ due to a source at the source point $\mathbf{r}_0$ is the same as the field u at the field point $\mathbf{r}_0$ due to a source at the source point $\mathbf{r}$. When the source and the receiver are interchanged, the matrix M_{ij} of the system changes. However, the resulting fields will be shown numerically to satisfy the principle of reciprocity.

In § 2 the problem is formulated and a dual series equation set is obtained. In § 3 the dual series equation set corresponding to the static problem is solved by making the direct transposition from the dual series problem to an equivalent integral equation (see (3.8) below) whose solution is known from [1]. The static solution is used in § 4 to obtain an equivalent dual series equation set ((4.1) and (4.2) below) whose properties are better suited for numerical implementation. A similar approach has been used in [2] for a different problem. It is shown that the reciprocity relation (interchange of source and receiver) is satisfied by the numerical solution. Examples of the field patterns induced near the dielectric semi-cylinder and the resulting bistatic radar cross sections are also given to demonstrate the efficacy of the solution.

2. Formulation. We consider the steady state problem of the scattering of waves emanating from a point source by a dielectric half-cylinder. See Fig. 1. We normalize the coordinates by the radius a of the half-cylinder. Space is divided into three regions: the region 1, which is the dielectric half-cylinder ($r < 1, |\theta| \in [\pi/2, \pi]$); the region 2, which is the complementary empty half-cylinder ($r < 1, \theta \in [-\pi/2, \pi/2]$); and the

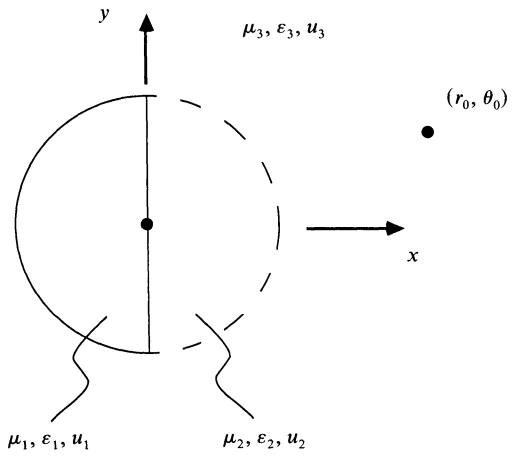

FIG. 1. *Geometry of the semi-cylinder scattering problem. Space is divided into three regions, each with its own physical characteristics. The source is assumed exterior to the cylinder radius.*

region 3, which excludes those cylinders ($r>1$, $\theta\in[-\pi, \pi]$). The fields, electric permittivity, and magnetic permeability are labeled, respectively, u_i, ε_i, and μ_i; $i=1, 2, 3$, with the understanding that $\varepsilon_2=\varepsilon_3$ and $\mu_2=\mu_3$.

We divide the problem into a symmetric problem (denoted by a superscript +) and an antisymmetric problem (denoted by a superscript −). Then the fields u_i shown in Fig. 1 are related to $u_i^{\pm}$ by

$$u_i = u_i^+ + u_i^-, \tag{2.1}$$

where

$$u_i^{\pm}(r, \theta) = \pm u_i^{\pm}(r, -\theta). \tag{2.2}$$

The governing differential equations and boundary conditions are

$$\Delta u_i^{\pm} + k_i^2 u_i^{\pm} = 0, \qquad i=1, 2, \quad r<1, \tag{2.3}$$

$$\Delta u_3^{\pm} + k_2^2 u_3^{\pm} = -\tfrac{1}{2}[\delta(\mathbf{r}-\mathbf{r}_0) \pm \delta(\mathbf{r}-\mathbf{r}_0^*)], \qquad r>1, \quad r_0>1, \tag{2.4}$$

$$u_1^{\pm}\left(r, \frac{\pi}{2}\right) = u_2^{\pm}\left(r, \frac{\pi}{2}\right), \qquad 0<r<1, \tag{2.5}$$

$$\partial_\theta u_1^{\pm}\left(r, \frac{\pi}{2}\right) = \eta \partial_\theta u_2^{\pm}\left(r, \frac{\pi}{2}\right), \qquad 0<r<1, \tag{2.6}$$

$$u_3^{\pm}(1, \theta) = H\left(\frac{\pi}{2}-\theta\right) u_2^{\pm}(1, \theta) + H\left(\theta-\frac{\pi}{2}\right) u_1^{\pm}(1, \theta), \qquad 0<\theta<\pi, \tag{2.7}$$

$$\partial_r u_3^{\pm}(1, \theta) = H\left(\frac{\pi}{2}-\theta\right) \partial_r u_2^{\pm}(1, \theta) + \eta^{-1} H\left(\theta-\frac{\pi}{2}\right) \partial_r u_1^{\pm}(1, \theta), \qquad 0<\theta<\pi, \tag{2.8}$$

where $k_i=(\varepsilon_i\mu_0)^{1/2}\omega/(ac)$ is the dimensionless wave number, $\eta=\varepsilon_1/\varepsilon_2$ is the ratio of the dielectric constants, $H(\theta)$ is the Heaviside function, and $\mathbf{r}_0^*=(r_0, -\theta_0)$ is the image of the source point $\mathbf{r}_0=(r_0, \theta_0)$. Also ω is the circular frequency (an $e^{+i\omega t}$ time dependence is assumed throughout), μ_0 is the dielectric permeability of free space, and c is the speed of light.

In the following, we only consider the symmetric problem and, for simplification of notation, we drop the superscript + on u_i^+ everywhere.

We now take

$$u_1 = \frac{4\eta}{\pi(3\eta+1)^{1/2}} \sum_{n=0}^{\infty} \left\{1+\frac{1}{2}\delta_{n0}(1+\eta^{-1})\right\} b_n v_n(r, \theta, k_1) + \frac{4\eta}{\pi(\eta+3)^{1/2}} \sum_{n=0}^{\infty} a_n w_n(r, \theta, k_1), \tag{2.9}$$

$$u_2 = \frac{4\eta}{\pi(3\eta+1)^{1/2}} \sum_{n=0}^{\infty} \left\{1+\frac{1}{2}\delta_{n0}(1+\eta^{-1})\right\} b_n v_n(r, \theta, k_2) + \frac{4}{\pi(\eta+3)^{1/2}} \sum_{n=0}^{\infty} a_n w_n(r, \theta, k_2), \tag{2.10}$$

$$u_3 = \sum_{n=0}^{\infty} (2-\delta_{n0}) \cos n\theta \left\{ C_n H_n(k_2 r) + \frac{i}{4} J_n(k_2 r) H_n(k_2 r_0) \cos n\theta_0 \right\}, \qquad r < r_0, \tag{2.11}$$

where δ_{ij} denotes the Kronecker delta function; H_n, the outgoing Hankel function of order n; J_n, the Bessel function of the first kind of order n, and

$$v_n(r, \theta, k) = \sum_{m=0}^{\infty} \beta_m^n(k)(-1)^{n+m} J_{2(m+n)}(kr) \cos(2(m+n)\theta), \tag{2.12}$$

$$w_n(r, \theta, k) = \sum_{m=0}^{\infty} \alpha_m^n(k)(-1)^{n+m} J_{2(m+n)+1}(kr) \cos((2m+2n+1)\theta), \tag{2.13}$$

$$\beta_m^n(k) = \left(\frac{2}{k}\right)^{2n} \frac{2(n+m)(2n+m-1)!}{m!}, \tag{2.14a}$$

$$\beta_0^0(k) = 1, \tag{2.14b}$$

$$\alpha_m^n(k) = \left(\frac{2}{k}\right)^{2n+1} \frac{(2n+1)(2n+m)!}{m!}. \tag{2.15}$$

For $r > r_0$, u_3 is given by (2.11), with r and r_0 interchanged in the second term under the summation.

The u_i as defined by (2.9)-(2.11) satisfy (2.3) and (2.4). Also, since

$$r v_n\left(r, \frac{\pi}{2}, k\right) = -(2n+1)^{-1} \partial_\theta w_n\left(r, \frac{\pi}{2}, k\right) = r^{2n+1}, \tag{2.16}$$

$$\partial_\theta v_n\left(r, \frac{\pi}{2}, k\right) = w_n\left(r, \frac{\pi}{2}, k\right) = 0, \tag{2.17}$$

we see that boundary conditions (2.5) and (2.6) are satisfied. Then substituting (2.9) into the remaining boundary conditions, (2.7) and (2.8), and operating on the result with $\int_0^\pi d\theta \cos n\theta$ yields

$$\pi\left\{C_n H_n(k_2)+\frac{i}{4}J_n(k_2)H_n(k_2 r_0)\cos n\theta_0\right\}$$

$$(2.18)\qquad =\int_0^{\pi/2}\cos(n\theta)u_2(1,\theta)\,d\theta+\int_{\pi/2}^{\pi}\cos(n\theta)u_1(1,\theta)\,d\theta,\qquad n=0,1,\cdots,$$

$$k_2\pi\left\{C_n H_n'(k_2)+\frac{i}{4}J_n'(k_2)H_n(k_2 r_0)\cos n\theta_0\right\}$$

$$(2.19)\qquad =\int_0^{\pi/2}\cos(n\theta)\partial_r u_2(1,\theta)\,d\theta+\eta^{-1}\int_{\pi/2}^{\pi}\cos(n\theta)\partial_r u_1(1,\theta)\,d\theta,\qquad n=0,1,\cdots,$$

where the prime denotes the derivative of the function. We eliminate C_n from (2.18) and (2.19), substitute from (2.9), (2.10), (2.12), and (2.13), and perform the θ integrations to achieve

$$(2.20)\qquad \frac{2}{\pi}\lambda\sum_{n=0}^{\infty}\frac{(n+\frac{1}{2})a_n}{(n+\frac{1}{2})^2-j^2}+(1+\delta_{j0})b_j=(1+\delta_{j0})c_j,\qquad j=0,1,\cdots,$$

$$(2.21)\qquad a_j-\frac{2}{\pi}\lambda\sum_{n=0}^{\infty}\frac{n}{(j+\frac{1}{2})^2-n^2}b_n=d_j,\qquad j=0,1,\cdots,$$

where

$$(2.22)\qquad \lambda=\frac{1-\eta}{[(3+\eta)(1+3\eta)]^{1/2}},$$

$$(2.23)\qquad c_j=(-1)^j(1-\tfrac{1}{2}\delta_{j0})(3\eta+1)^{-1/2}q_{2j}\bar{H}_{2j}+\hat{H}_{2j}\hat{c}_j+\bar{c}_j,$$

$$(2.24)\qquad d_j=(-1)^j(3+\eta)^{-1/2}q_{2j+1}\bar{H}_{2j+1}+\hat{H}_{2j+1}\hat{d}_j+\bar{d}_j,$$

$$q_0=\tfrac{1}{2}i\pi-\gamma_e-\log(\tfrac{1}{2}k_2),\qquad \gamma_e=0.577\cdots\ \text{(Euler's constant)},$$

$$q_j=\frac{1}{j},\qquad j>0,$$

$$\bar{H}_j=\frac{1}{2}\left[\frac{H_j(k_2r_0)}{H_j(k_2)}\right]\cos(j\theta_0),$$

$$\hat{H}_j=1+q_jk_2\left[\frac{H_j'(k_2)}{H_j(k_2)}\right],$$

$$\hat{c}_j=\frac{\eta}{(3\eta+1)}\sum_{n=0}^{j}b_n\left[1+\frac{1}{2}\delta_{n0}(1+\eta^{-1})\right][\beta_{j-n}^n(k_2)J_{2j}(k_2)+\beta_{j-n}^n(k_1)J_{2j}(k_1)]$$

$$+\frac{\lambda(2-\delta_{j0})}{\pi(1-\eta)}\sum_{n=0}^{\infty}\sum_{m=0}^{\infty}\frac{(m+n+\frac{1}{2})a_n}{(m+n+\frac{1}{2})^2-j^2}$$

$$\cdot\{\alpha_m^n(k_2)J_{2m+2n+1}(k_2)-\eta\alpha_m^n(k_1)J_{2m+2n+1}(k_1)\},$$

$$\bar{c}_j = -\hat{c}_j + b_j + \lambda\pi^{-1}(2-\delta_{j0}) \sum_{n=0}^{\infty} \frac{(n+\frac{1}{2})a_n}{(n+\frac{1}{2})^2 - j^2}$$

$$-\frac{\eta q_{2j}}{(3\eta+1)} \sum_{n=0}^{j} b_n \left[1 + \frac{1}{2}\delta_{n0}(1+\eta^{-1})\right]$$

$$\cdot [k_2 \beta_{j-n}^n(k_2) J'_{2j}(k_2) + \eta^{-1} k_1 \beta_{j-n}^n(k_1) J'_{2j}(k_1)]$$

$$-\frac{\lambda q_{2j}(2-\delta_{j0})}{\pi(1-\eta)} \sum_{n=0}^{\infty} \sum_{m=0}^{\infty} \frac{(m+n+\frac{1}{2})a_n}{(m+n+\frac{1}{2})^2 - j^2}$$

$$\cdot \{k_2 \alpha_m^n(k_2) J'_{2m+2n+1}(k_2) - k_1 \alpha_m^n(k_1) J'_{2m+2n+1}(k_1)\},$$

$$\bar{d}_j = -\hat{d}_j + a_j - \frac{2}{\pi}\lambda \sum_{n=1}^{\infty} \frac{n b_n}{(j+\frac{1}{2})^2 - n^2}$$

$$-\frac{q_{2j+1}}{(3+\eta)} \sum_{n=0}^{j} a_n \{k_2 \alpha_{j-n}^n(k_2) J'_{2j+1}(k_2) + k_1 \alpha_{j-n}^n(k_1) J'_{2j+1}(k_1)\}$$

$$-\frac{2\eta\lambda}{\pi(1-\eta)} q_{2j+1} \sum_{n=0}^{\infty} \sum_{m=0}^{\infty} \frac{b_n[1+\frac{1}{2}(1+\eta^{-1})\delta_{n0}][j+\frac{1}{2}]}{(j+\frac{1}{2})^2 - (m+n)^2}$$

$$\cdot \{k_2 \beta_m^n(k_2) J'_{2(m+n)}(k_2) - \eta^{-1} k_1 \beta_m^n(k_1) J'_{2(m+n)}(k_1)\},$$

$$\hat{d}_j = (3+\eta)^{-1} \sum_{n=0}^{j} a_n \{\alpha_{j-n}^n(k_2) J_{2j+1}(k_2) + \eta \alpha_{j-n}^n(k_1) J_{2j+1}(k_1)\}$$

$$+\frac{2\eta\lambda}{\pi(1-\eta)} \sum_{n=0}^{\infty} \sum_{m=0}^{\infty} \frac{b_n[1+\frac{1}{2}(1+\eta^{-1})\delta_{n0}](j+\frac{1}{2})}{(j+\frac{1}{2})^2 - (m+n)^2}$$

$$\cdot \{\beta_m^n(k_2) J_{2(m+n)}(k_2) - \beta_m^n(k_1) J_{2(m+n)}(k_1)\}.$$

We now discuss (2.20) and (2.21), which determine a_j and b_j. With c_j and d_j defined by (2.23) and (2.24), we observe that as k_1 and k_2 go to 0, $\hat{H}_j$, $\bar{c}_j$, and $\bar{d}_j$ all go to 0. Thus the left-hand sides of (2.20) and (2.21) represent the static limit of this problem. As j goes to infinity, $\hat{H}_j$ is $O(1/j)$ and the quantities $\bar{c}_1$ and $\bar{d}_j$ are $O(1/j)$ with respect to the left-hand sides of (2.20) and (2.21). We take advantage of this result in § 4, where we describe our numerical method of solution.

3. Solution to the static problem. In this section we solve the dual series (2.20) and (2.21) for a_j and b_j, treating c_j and d_j as known quantities. Also, we discuss the behavior near the corner. In lieu of the dual series, we consider instead

$$\lambda A(\xi) + B(\xi) = 0, \qquad |\xi| < 1, \tag{3.1}$$

$$\int_{-1}^{1} [(1-\zeta^2)^{1/2} A(\zeta) - \lambda(1-\xi^2)^{1/2} B(\zeta)] \frac{d\zeta}{\xi - \zeta} = Q(\xi), \qquad |\xi| < 1, \tag{3.2}$$

where

$$A(\xi) = \sum_{n=0}^{\infty} a_n U_{2n}(\xi), \tag{3.3}$$

$$B(\xi) = \sum_{n=0}^{\infty} (b_n - c_n) T_{2n}(\xi)(1-\xi^2)^{-1/2}, \tag{3.4}$$

$$Q(\xi) = \pi \sum_{n=0}^{\infty} [d_n T_{2n+1}(\xi) - \lambda c_{n+1} U_{2n+1}(\xi)(1-\xi^2)^{1/2}], \tag{3.5}$$

and T_n and U_n denote the Chebyshev polynominals of the first and second kind, respectively.

Operating on (3.1) with

$$\int_{-1}^{1} d\xi\, T_{2j}(\xi)$$

yields (2.20), and operating on (3.2) with

$$\int_{-1}^{1} d\xi (1-\xi)^{-1/2} T_{2j+1}(\xi)$$

yields (2.21). Thus, knowing the solution to (3.1) and (3.2), we obtain the solution to (2.20) and (2.21) from

$$a_j = \frac{2}{\pi} \int_{-1}^{1} (1-\xi^2)^{1/2} U_{2j}(\xi) A(\xi)\, d\xi, \tag{3.6}$$

$$\begin{aligned} b_j &= c_j + \left(\frac{2-\delta_{j0}}{\pi}\right) \int_{-1}^{1} T_{2j}(\xi) B(\xi)\, d\xi \\ &= c_j - \lambda \left(\frac{2-\delta_{j0}}{\pi}\right) \int_{-1}^{1} T_{2j}(\xi) A(\xi)\, d\xi. \end{aligned} \tag{3.7}$$

Eliminating B from (3.1) and (3.2) yields the integral equation

$$(LA)(\xi) \equiv \int_{-1}^{1} [(1-\zeta^2)^{1/2} + \lambda^2 (1-\xi^2)^{1/2}] \frac{A(\zeta)\, d\zeta}{\xi - \zeta} = Q(\xi), \qquad |\xi| < 1. \tag{3.8}$$

This equation has been studied in detail by Gautesen [1]. We summarize his results as they apply to this work.

Upon examining (3.5)-(3.7), we see that we are only interested in certain moments of the solutions to

$$(LV_j)(\xi) = T_{2j+1}(\xi), \qquad |\xi| < 1, \tag{3.9}$$

$$(LW_j)(\xi) = (1-\xi^2)^{1/2} U_{2j+1}(\xi), \qquad |\xi| < 1. \tag{3.10}$$

They are

$$\begin{aligned} \int_{-1}^{1} (1-\xi^2)^{1/2} U_{2m}(\xi) V_j(\xi)\, d\xi &= \sum_{n=1}^{2j+1} (-1)^n \left(1 - \frac{1}{2}\delta_{n(2j+1)}\right) \sigma_{2j-n} \\ &\quad \cdot [\sigma_{2m+n} + \operatorname{sgn}(2m-n+1) \sigma_{|n-2m-1|-1} - 2\sigma_{2m}], \end{aligned} \tag{3.11}$$

$$\begin{aligned} |\lambda| \int_{-1}^{1} T_{2m}(\xi) V_j(\xi)\, d\xi &= \sum_{n=1}^{2j+1} (-1)^n \left(1 - \frac{1}{2}\delta_{n(2j+1)}\right) \sigma_{2j-n} \\ &\quad \cdot [\sigma_{2m+n-1} + \sigma_{|2m-n|-1} - 2\sigma_{2m-1}], \end{aligned} \tag{3.12}$$

$$\begin{aligned} 4\Lambda|\lambda| \int_{-1}^{1} (1-\xi^2)^{1/2} U_{2m}(\xi) W_j(\xi)\, d\xi \\ = \sum_{n=1}^{2j+2} (-1)^n \gamma_{2j+1-n} [(2m+n+2)\sigma_{2m+n+1} - |2m-n| \sigma_{|2m-n|-1} - 4\Lambda(n+1)\sigma_{2m}], \end{aligned} \tag{3.13}$$

$$\begin{aligned} 4\Lambda|\lambda|^2 \int_{-1}^{1} T_{2m}(\xi) W_j(\xi)\, d\xi &= \sum_{n=1}^{2j+2} (-1)^n \gamma_{2j+1-n} [(2m+n+1)\sigma_{2m+n} \\ &\quad + (n-2m+1)\sigma_{|2m-n-1|-1} - 4\Lambda(n+1)\sigma_{2m-1}], \end{aligned} \tag{3.14}$$

where $\operatorname{sgn}(0) \equiv 0$, $\sigma_{-2} = 0$, $\sigma_{-1} = 1$, $\sigma_0 = 2\Lambda$,

$$(n+2)\sigma_{n+1} = 4\Lambda\sigma_n + n\sigma_{n-1}, \qquad n = 0, 1, \cdots, \tag{3.15}$$

$$\gamma_n = (1 - \tfrac{1}{2}\delta_{1|n|})\sigma_{|n|-2} - \sigma_n, \qquad n = -1, 0, \cdots, \tag{3.16}$$

$$\Lambda = \frac{1}{\pi}\tan^{-1}\left(\frac{1}{|\lambda|}\right). \tag{3.17}$$

We remark that (3.15) is a stable three-term recurrence relation.

We now discuss the nature of the behavior near the corner for the static solution. In (2.20) and (2.21), let us take $c_j = 0$ and $d_j = \delta_{j0}$. The corresponding constants a_n and b_n are easily obtainable by the above results. In the static limits, (2.9) at $\theta = \pi/2$ becomes

$$u_1\left(r, \frac{\pi}{2}\right) = \frac{4\eta}{\pi(3\eta+1)^{1/2}} \sum_{n=0}^{\infty} \left\{1 + \frac{1}{2}\delta_{n0}(1+\eta^{-1})\right\} b_n r^{2n}. \tag{3.18}$$

Then using the relation

$$1 + 2\sum_{n=1}^{\infty} \sigma_{n-1} r^n = \left(\frac{1+r}{1-r}\right)^{2\Lambda} \equiv \phi(r), \tag{3.19}$$

we find that for this example

$$u_1\left(r, \frac{\pi}{2}\right) = \text{const} + (\text{const}) r^{-1}[(1-r)^2\phi(r) - (1+r)^2\phi(-r)]. \tag{3.20}$$

Thus near $r = 1$, the exponents of the singularities are 0, 2Λ, $2 - 2\Lambda$. These are the admissible singularities near the corner.

4. Numerical solution. In this section we describe our numerical procedure. We invert (2.20) and (2.21) as described in the previous section, and then substitute for c_j and d_j from (2.23) and (2.24). The result can be expressed as

$$a_j = c_j^1 + \sum_{n=0}^{\infty} [C_{jn}^{11} a_n + C_{jn}^{12} b_n], \qquad j = 0, 1, \cdots, \tag{4.1}$$

$$b_j = c_j^2 + \sum_{n=0}^{\infty} [C_{jn}^{21} a_n + C_{jn}^{22} b_n], \qquad j = 0, 1, \cdots, \tag{4.2}$$

where all quantities are known except a_j and b_j. The remark made at the end section of § 2 implies that the sums (4.1) and (4.2) are smaller than a_j and b_j for j sufficiently large. Therefore, this infinite system of equations can be truncated in order to obtain a numerical solution. This approximation leads to the solution system

$$a_j = c_j^1 + \sum_{n=0}^{N} [C_{jn}^{11} a_n + C_{jn}^{12} b_n], \qquad j = 0, 1, \cdots, N, \tag{4.3}$$

$$b_j = c_j^2 + \sum_{n=0}^{N} [C_{jn}^{21} a_n + C_{jn}^{22} b_n], \qquad j = 0, 1, \cdots, N, \tag{4.4}$$

which can then be solved numerically by inverting the resulting finite matrix for a_j and b_j, $j = 0, 1, \cdots, N$. For $j > N$, we simply use the relations

$$a_j = c_j^1 + \sum_{n=0}^{N} [C_{jn}^{11} a_n + C_{jn}^{12} b_n], \qquad j > N, \tag{4.5}$$

$$b_j = c_j^2 + \sum_{n=0}^{N} [C_{jn}^{21} a_n + C_{jn}^{22} b_n], \qquad j > N. \tag{4.6}$$

With these coefficients, we then use (2.9)-(2.11) to construct the H_z fields. Ampere's law may then be applied to yield the E_r and E_θ field components.

Several numerical tests were used to verify the accuracy of the solution. First and most obvious was to verify that the boundary conditions (2.4)-(2.8) were satisfied by the solution. Since conditions (2.4)-(2.6) were built into the solution basis functions, only (2.7) and (2.8) yield information on the solution process itself. Because these two conditions pertain to the continuity of the field and its derivative across $r = 1$, the solution was checked by examining the fields at $r = 1_-$ and $r = 1_+$.

Once the boundary conditions were verified, the results were numerically tested as a solution to the original differential equation (2.4). This was done by writing a procedure to numerically produce the required derivatives and substitute them into (2.3). Having verified that the numerical results satisfy the boundary conditions and satisfy the differential equation, we know that the solution is the correct one because the uniqueness theorem guarantees it.

To obtain a quantitative estimate of the accuracy of the solution, we tested its satisfaction of the principle of reciprocity. A typical result is shown in Fig. 2, for the case in which the dielectric ratio $\eta = 3$ and the characteristic value $ka = 0.36$. We solved for $N = 95$ solution coefficients in this case. The test utilized eight receiver points along the x axis between $x = 1.21$ and $x = 1.56$ and the source also on this axis at ($x = 5.0$, $y = 0.0$). The source and receiver points were then interchanged. We have graphed the differences between the field values in these two reciprocal configurations for all of the points considered. The differences are negligible. Because it is a stringent test of the solution, the reciprocity test has been incorporated as a standard test of the solution quality, i.e., of the number of solution coefficients required, whenever new values of ka are considered.

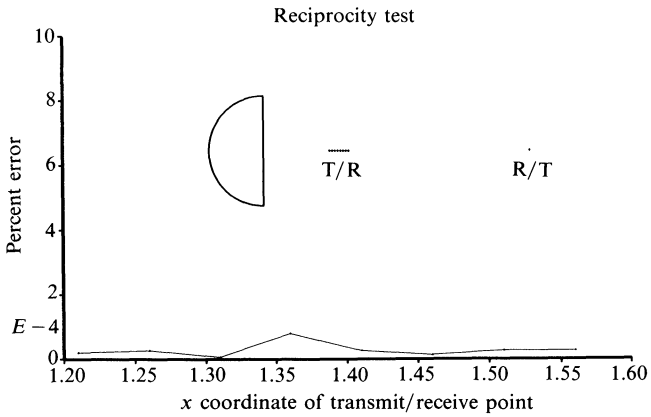

FIG. 2. *The reciprocity relation is satisfied by the semi-cylinder solution. The difference between the field values obtained from interchanging the source and transmitter is shown relative to the distance of the original source locations from the origin.*

The various field components are obtained once the solution coefficients have been generated. We show, respectively, in Figs. 3(a) and 3(b), the total E_r and H_z field components induced near a dielectric semi-cylinder with the dielectric ratio $\eta = 3$ by a point source located along the x axis at ($x = 5.0$, $y = 0.0$). The characteristic value $ka = 2.00$, and $N = 380$ solution coefficients were employed. Note that since the source is on the axis, the symmetric solution obtained here is the complete result.

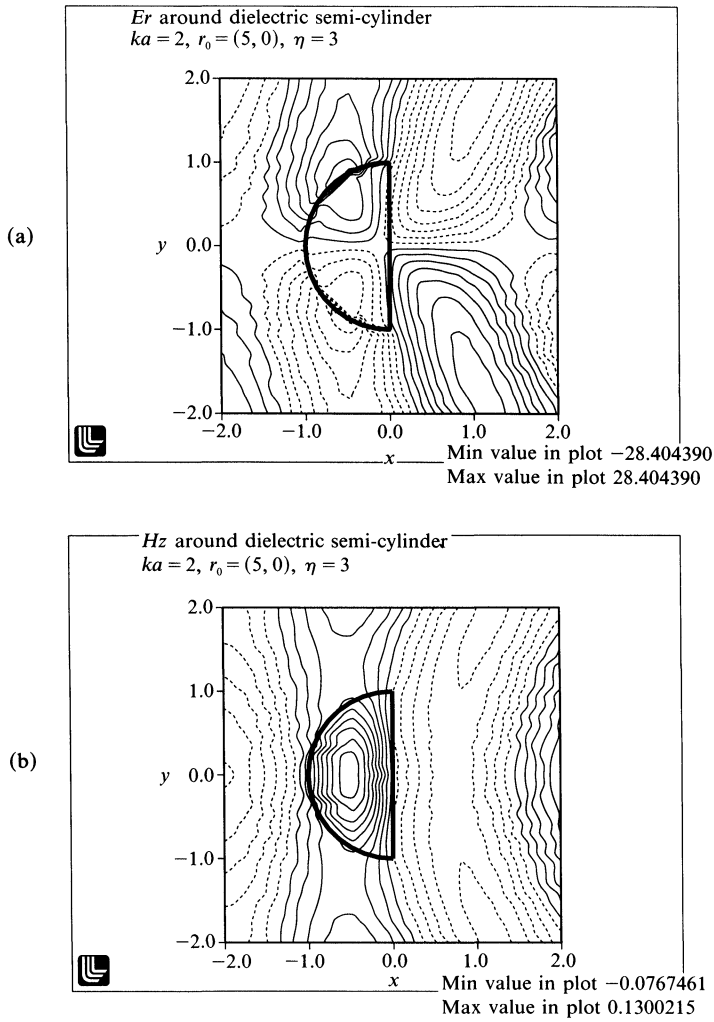

FIG. 3. *The field components are generated once the solution coefficients are obtained. The total E_r and H_z field components induced near a dielectric semi-cylinder with the dielectric ratio $\eta = 3$ by a point source along the x axis at $(x = 5.0, y = 0.0)$ are shown, respectively, in* (a) *and* (b). *The characteristic value $ka = 2.00$.*

In Figs. 3(a) and 3(b), the solid lines represent positive field values, the dashed lines negative values. We can clearly see the localization of the H_z field contours in the dielectric in Fig. 3(b). The lens effect of the semi-cylinder which transforms the cylindrical wave of the point source to more of a plane wave character can also be perceived. The discontinuities in the normal field component E_r across the dielectric interfaces are also clearly seen in Fig. 3(a).

Another scattering quantity of interest is the bistatic radar cross section. For the present problem, it is defined as

$$\sigma(\theta, \theta_0) = \lim_{r\to\infty}\left[2\pi r \frac{|H_z^{\text{scat}}(r, \theta)|^2}{|H_z^{\text{inc}}(\vec{r} = 0)|^2}\right]. \tag{4.7}$$

It reduces to the expression

$$\sigma(\theta, \theta_0) = \frac{64}{k_2}\left[\frac{|S(\theta, \theta_0)|^2}{|H_0(k_2 r_0)|^2}\right], \tag{4.8}$$

where we have the term

$$S(\theta, \theta_0) = \sum_{n=0}^{\infty} (2 - \delta_{on})\, e^{-in\pi/2} \cos n\theta\, C_n. \tag{4.9}$$

This defines the bistatic radar cross section in terms of the exterior region solution coefficients. The bistatic radar cross section for the case corresponding to Figs. 3(a) and 3(b) is given in Fig. 4. It shows the enhancement of the field in the forward scattering direction by the semi-cylinder "lens." The side lobes in the radar cross section are aligned with the field modes seen in Figs. 3(a) and 3(b). It also shows the expected symmetry of the far-field about the source/semi-cylinder axis.

As the values of ka are increased, we can observe the transition between the different allowed modes of the solution in the field contour plots. This information can then be correlated with the bistatic radar cross section to determine the influence on the far-field behavior of variations in the dielectric parameters. This is particularly true for the influence of the dielectric corners on the far-field of the resulting fields.

5. Discussion. We have presented a dual series solution to the electromagnetic semi-cylinder scattering problem. The complete problem was decomposed into its symmetric and antisymmetric components. Only the symmetric part was solved explicitly. The antisymmetric problem solution follows immediately in an analogous fashion and has been left to future efforts.

We have assumed throughout that $r_0 > 1$. If $r_0 < 1$, then the source term in the right side of (2.4) is replaced by 0 and the second term under the summation in (2.11) is omitted. The source term would then appear in the right side of (2.3) as

$$-\tfrac{1}{2}[\delta(\mathbf{r} - \mathbf{r}_0) \pm \delta(\mathbf{r} - \mathbf{r}_0^*)]\delta_{ij},$$

where $j = 1$ if the source is inside the dielectric half-cylinder or $j = 2$ if the source is outside of it. Then to the field u_j we would add the source term

$$\frac{i}{4} \sum_{n=0}^{\infty} (2 - \delta_{n0}) J_n(k_j r_<) H_n(k_j r_>) \cos n\theta \cos n\theta_0,$$

where $r_< = \min(r, r_0)$ and $r_> = \max(r, r_0)$. In (4.1) and (4.2) the changes would only appear in the inhomogeneous terms c_j^1 and c_j^2.

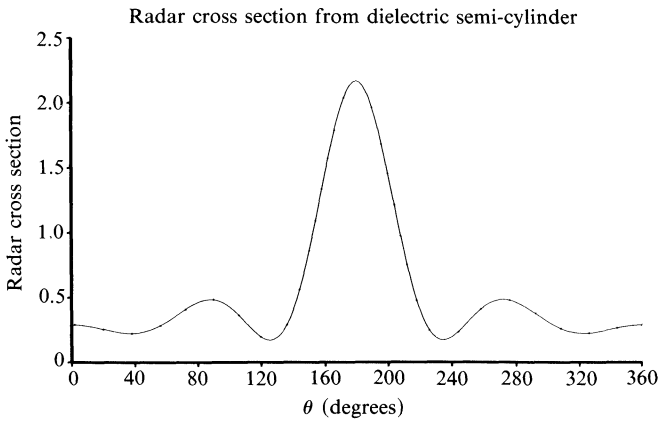

FIG. 4. *The bistatic radar cross section is generated once the solution coefficients are obtained. The bistatic radar cross section resulting from the field which originates from a point source along the x axis at* ($x = 5.0$, $y = 0.0$) *and is scattered by a dielectric semi-cylinder with the dielectric ratio* $\eta = 3$ *is shown. The characteristic value* $ka = 2.00$.

As with any solutions to canonical problems, their complete usefulness is only realized after exercising them for many different cases. One area of interest would be for the application of the solution to the Geometric Theory of Diffraction [6] class of solutions. We have begun a study of the problem solution with the hope of extracting the diffraction coefficient, at least presently, for the restricted geometry where the point source is on the x axis. The general diffraction coefficient will await the completed implementation of the general problem's solution.

REFERENCES

[1] A. K. GAUTESEN, *The effective conductivity of a composite material with periodic rectangular geometry*, SIAM J. Appl. Math., 48 (1988), pp. 393–404.

[2] R. W. ZIOLKOWSKI, *n-series problems and the coupling of electromagnetic waves to apertures: A Riemann–Hilbert approach*, SIAM J. Math. Anal., 16 (1985), pp. 358–378.

[3] J. VAN BLADEL, *Field singularities at metal-dielectric wedges*, IEEE Antennas and Propagat., AP-33 (1985), pp. 450–455.

[4] J. MEIXNER, *The behavior of electromagnetic fields at edges*, IEEE Antennas and Propagat., AP-20 (1972), pp. 442–446.

[5] J. B. ANDERSON, *Field behavior near a dielectric wedge*, IEEE Antennas and Propagat., AP-26 (1978), pp. 598–602.

[6] J. B. KELLER, *Geometrical theory of diffraction*, J. Opt. Soc. Amer., 52 (1962), pp. 116–130.